Autonomous Over-The-Horizon Rover Navigation

Erick Dupuis, Ioannis Rekleitis, Jean-Luc Bedwani, David Gingras
Pierre Allard, Tom Lamarche,
Wen-Hong Zhu
Canadian Space Agency[1]
erick.dupuis@space.gc.ca

Abstract

This paper presents results from the 2006 and 2007 test campaigns of the Canadian Space Agency's autonomous rover navigation research. In particular, results are provided in the area of terrain modelling, path planning and 3D odometry. Results are also provided for integrated system tests whereby the rover travelled autonomously and semi-autonomously beyond its sensing horizon. It provides a summary of the experimental results that were obtained through two seasons of test campaigns.

1. Introduction

Mobile robotics has enabled scientific breakthroughs in planetary exploration [1]. The Mars Exploration Rovers (MERs) "Spirit" and "Opportunity" have made discoveries that were only enabled by their to ability to move around the surface of Mars: sampling rock outcrops, examining rocks samples and descending into craters. Both of these rovers have the ability to detect and avoid obstacles, picking a path that would take them along a safe trajectory. On occasion, the rovers have had to travel to locations that were at the fringe of the horizon of their sensors or even slightly beyond.

The next rover missions to Mars are the "Mars Science Laboratory" (MSL) [2] and ESA's ExoMars [3]. Both of these missions have set target traverse distances on the order of one kilometre per day. Both the MSL and ExoMars rovers are therefore expected to drive regularly a significant distance beyond the horizon of their environment sensors. Earth-based operators will therefore not know a-priori the detailed geometry of the environment and will thus not be able to select via-points for the rovers throughout their traverses.

Some of the key technologies that will be required are the ability to sense and model the 3D environment to plan paths through it and to autonomously navigate along those paths. To address the above mentioned issues, the Canadian Space Agency is developing a suite of technologies for long-range rover navigation. For the purposes of this paper, "long-range" is defined as a traverse that takes the rover beyond the horizon of the rover's environment sensors.

This paper provides a summary of the experimental results that were obtained through two seasons of test campaigns. In particular, results are provided in the area of terrain modelling, path planning and 3D odometry. Results are also provided for integrated system tests whereby the rover travelled autonomously and semi-autonomously beyond its sensing horizon.

2. Review of Existing Work

Currently, the most advanced exploration robots that have been deployed for planetary exploration are the Mars Exploration Rovers (MER) "Spirit" and "Opportunity". These rovers have successfully demonstrated, on Mars, concepts such as visual odometry and autonomous path selection from a terrain

model acquired from sensor data [4]. The main sensor suite used for terrain assessment for the MER has been passive stereo vision [5]. The models obtained through stereo imagery are used for both automatic terrain assessment and visual odometry.

Automatic terrain assessment is done using the cloud of 3D points in front of the rover to evaluate the traversability of the terrain, defined as a regular grid of square patches. Visual odometry used stereo camera views to identify and track features of the terrain to mitigate the effect of slip [1]. Due to high computation load visual odometry is rarely used on the MERs, a more efficient algorithm is proposed for the Mars Science Laboratory mission planned for 2010 [6].

The problem of autonomous long range navigation is also very important in terrestrial settings. As an example, the DARPA grand challenge in 2005 resulted in several vehicles travelling autonomously 132 miles over desert terrain [7]. Another example of integrated autonomous navigation experiments is the scientific rover campaigns conducted in the Atacama Desert where traverses on the order of 30Km were conducted [8]. An excellent discussion on the issues that need to be resolved for autonomous navigation in natural setting can be found in [9].

Some of the most important choices for autonomous rover navigation are the sensing modality used and the environment representation. Both vision [10][11][12] and LIDAR [13][14] technologies have been proposed, each one having different advantages and disadvantages. Early work on planetary exploration using LIDAR, though promising, was not compatible with the weight constraints. The Mars Exploration Rovers are currently performing long traverses using passive stereo vision [15]. Stereo vision although lightweight, requires more computing power, has limited range and accuracy. Currently, laser-based systems such as LIDAR have been successfully used in space mission such as XSS-11, Phoenix and on the Space Shuttle Program (Orbiter Boom Sensor System) and thus are space qualified. The major advantage of laser systems is their superior resolution and range.

3. Research Objectives

The goal of our work is to navigate autonomously from the current position to an operator-specified location which lies beyond the sensing horizon of the rover. In order to achieve this goal several components need to be developed, tested and integrated. Figure 1 presents a schematic diagram of the different components. We operate under the assumption that a global map is available from satellite imagery, previous missions, or from data collected during descent.

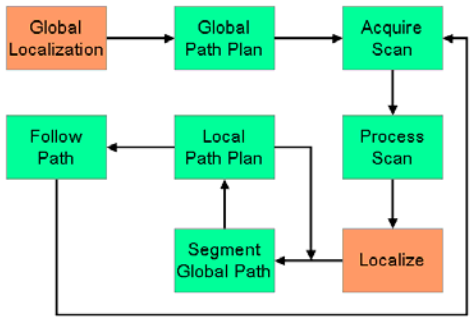

Figure 1 - Autonomous navigation process flow diagram

The rover uses the global map to plan a path from its current position to the operator-specified location; the rover collects the first local scan using its LIDAR sensor, then the global path is segmented successively using the locally collected scans, each time a refined path is planned through the local scan. The rover uses the local path to navigate to the next way-point.

At the current state, the pose estimation from the IMU and the odometer, allows to safely navigate along trajectories on the order of tens of meters without re-localizing between successive scans. As traverse lengths increase, localisation will become essential. However, preliminary test results of the localisation schemes developed so far, though promising, have not yet proven to be robust enough.

The main aspects on which our research has concentrated are in the area of terrain modelling, path planning and 3D odometry. The terrain modelling scheme is centered on the Irregular Triangular Mesh (ITM) [17] representation of the terrain that can be obtained from the LIDAR point cloud. The ITM representation has several desirable properties: it can use the LIDAR data directly as an input source and it is directly amenable to graph search path planning techniques. One of its main advantages is its potential for developing memory-efficient terrain models. Indeed, ITM terrain models can easily be compressed using information-preserving algorithms by removing co-planar triangles, thus drastically reducing the memory occupied by the terrain model. [18]

Another aspect of our research has been the usage of the ITM representation for graph search path planning techniques. The triangular cells in the ITM are converted in a graph where neighbourhood

relationships between cells for the edges of the graph. The results presented in this paper are based on techniques such as Dijkstra's graph search and A*. The latest version of the planner that was used is based on the A* algorithm using cost functions that take into account the physical dimensions and terrain climbing capabilities of the rover. [19]

Another interesting aspect of the research described in this paper is directly related to fact that visual odometry cannot be used due to the absence of stereo cameras on-board the rover. All terrain modelling is based on terrain scans taken at discrete times. Localisation must therefore be based on terrain model matching [20] and sensor fusion is used to ensure highly accurate 3D odometry based on the fusion of inertial, heading and wheel odometry sensor readings.

4. Experimental Test-bed

The experiments described in this paper were conducted in the CSA's Mars Emulation Terrain: a 30m x 60m that emulates a broad variety of Martian topographies. The mobile robot base that was used to conduct the experiments is a P2-AT mobile robot from ActiveMedia (see Figure 2). It is equipped with sonar sensors for obstacle detection, a 6-axis inertial measurement unit and a digital compass.

Different sensors have been mounted on the rover for 3D environment sensing: during the 2006 test campaign, the sensor that was used was an ILRIS 3D LIDAR surveying LIDAR from Optech. The ILRIS uses a scanning pulsed laser to measure distance based on the time of flight of the laser beam. The raw data provided by the sensor is a 3D point cloud. It has a measurement range from 3 meters to over 1.5 km. It provides measurements with range accuracy on the order of 1 cm over its entire range. Its field of view is 40 degrees by 40 degrees and it scans approximately 2000 points per second.

For the 2007 test campaign, the ILRIS was replaced by a SICK LMS-200 Laser range scanner. The LMS-200 sensor provides a line scan over a range of up to 80 meters with resolution between 0.25 and 1.0 degree and a field-of-view of 180 degrees. Mounting the SICK sensor such that the laser stripe is vertical on a turntable has allowed us to obtain full 360 degree coverage around the rover.

Figure 2 - CSA's Mobile Robotics Test-bed

5. Experimental Results

The experimental results presented in the following sections have been acquired through two successive seasons of rover testing. Where applicable, comparative results between the two testing seasons are presented in order to appreciate the strengths of one method or rover configuration over another.

5.1. Terrain Modelling

The performance of the decimation algorithms used for terrain modelling have been tested using the data acquired during every experiment run in the 2006 and 2007 test seasons. In total 195 scans of terrain representative of the Martian surface have been used to characterise the performance of the algorithms.

The LIDAR point clouds were fed off-line to the terrain modelling algorithm. For each data set, the point cloud was meshed to obtain an un-decimated ITM. The mesh was then compressed using different decimation targets. In 2006, target decimation ratios ranged from 80% to 95% (removing between 80% and 95% of the original number of cells in the model). For each scan, the decimation stopped either when attaining the desired decimation ratio or when the error between the decimated model and the original point cloud exceeded a given error threshold (1.5 cm). In 2007, the increase in the field-of-view dramatically increased the number of points in the raw scan. This prompted the addition of an additional decimation target at 99%.

Table 1 shows a comparison of the performance statistics of the decimation algorithm on the LIDAR scans. Note the increase in the number of cells in the scan due to the increase of the field of view for the 2007 data. The results from the 2007 test season show that, on average, it is possible to decimate representative terrain scans by a factor near 97%

leading to terrain models containing on the order of 6500 cells from point clouds that contained more than 200 000 cells in raw form. The decimated model preserves geometric information of the terrain since the maximum error for all of these tests was limited to 1.5 cm.

Figure 3 shows decimated scans from the ILRIS-3D sensor and from the SICK LMS sensor. Subfigures (a) and (d) show the raw point clouds, (b) and (e) show the results of a Delaunay mesh of the raw point cloud, and (c) and (f) show decimated meshes.

Table 1 - Decimation Test Results

			# Cells in Raw Scan	Target Decimation Ratio			
				80%	90%	95%	99%
2006	Number of Cells		61670	12333	6194	3591	-
	Effective Decimation Ratio	Mean	-	80.00%	89.91%	94.01%	-
		Std Dev	-	0.00%	0.75%	1.90%	-
2007	Number of Cells		216361	43272	21635	10858	6412
	Effective Decimation Ratio	Mean	-	80.0%	90.0%	94.98%	97.04%
		Std Dev	-	0.00%	0.00%	0.14%	1.20%

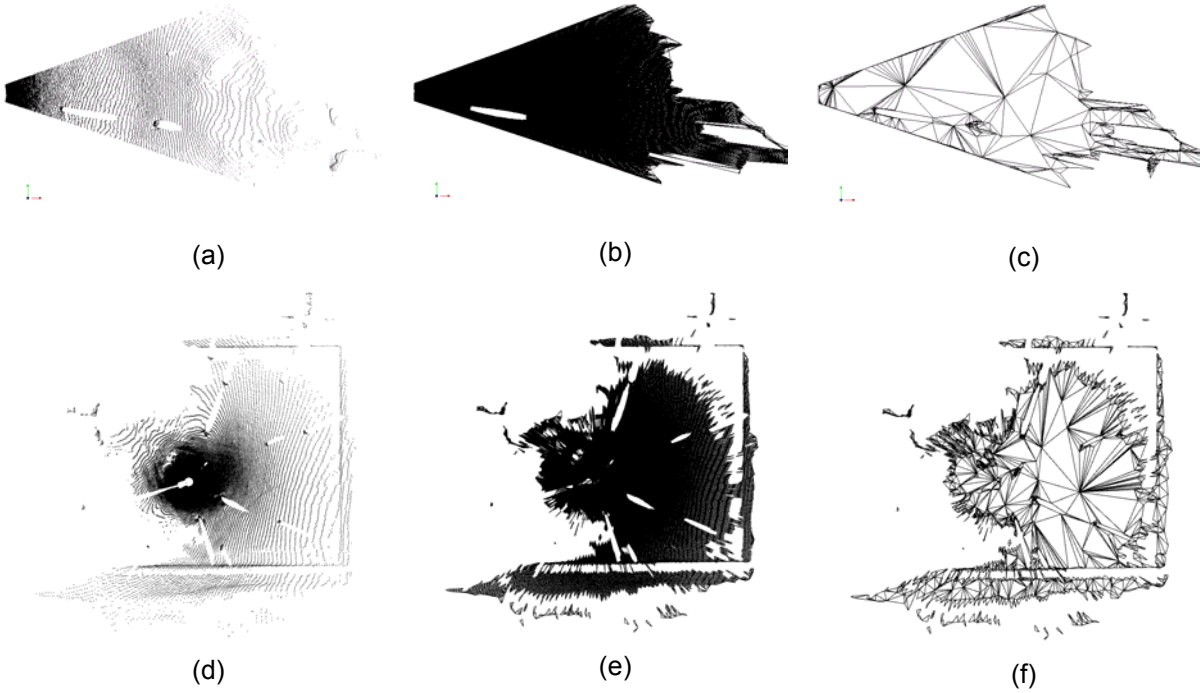

Figure 3 - Terrain Modelling: (a) Raw point cloud from ILRIS-3D, (b) Delaunay Mesh of the Raw Data, (c) Decimated Mesh, (d) Raw Point Cloud of the Scanning SICK, (d) Delaunay Mesh of the Raw Data, (f) Decimated Mesh

5.2. Path Planning

The performance of the path planning algorithms was also tested off-line using the full data sets acquired in 2006 and in 2007. Since major improvements were implemented in between the two test seasons, only the results of the 2007 field-testing season are presented here. An integrated test methodology was used to assess the performance of the planner over local terrain models and global terrain models at the same time. For each test, the terrain scan was geo-localised on the global terrain model. A target destination was given beyond the horizon of local scan, typically at the other end of the terrain. The planner was then invoked on a decimated model of the Mars Emulation Terrain. The resulting global path was then segmented by selecting a maximum radius and the planner was invoked on the local terrain scan. The planner succeeded in finding feasible paths for 100% of the test cases. Figure 4 shows a typical output from one of the off-line path planning tests. The local scan is overlaid on the global terrain model. The path segmentation algorithm automatically picked an attainable point in the close vicinity of the global path and within the shaded area.

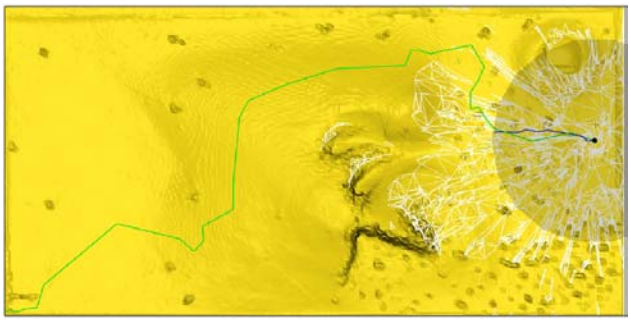

Figure 4 - Results of Planning Experiment. Global Path is green, Local Path is blue. Shaded area delimits Local Planning Horizon

The results of the off-line planning experiments on the 2006 and 2007 data showed that the planner successfully found safe paths in 100% of the cases where a path existed. The 2007 tests further demonstrated that the path segmentation algorithm also functioned. Figure 5 and Figure 6 show the statistical distribution of computing time for the global planning process and the local planning process on the 2007 data set. The computer used for these tests was a Dual Core 2.0 GHz laptop computer running the Linux operating system. Given that the planner was operating on models with approximately 6000 cells, the planning time is acceptable.

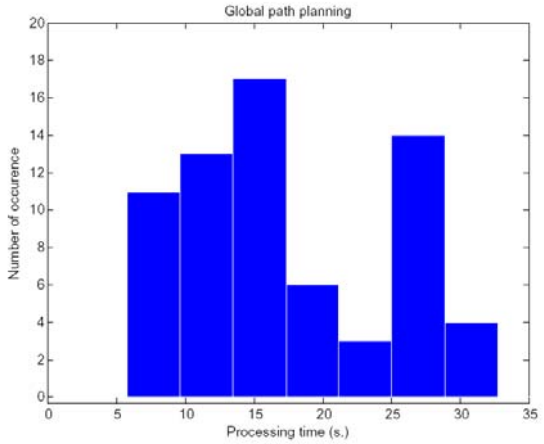

Figure 5 - Statistical Distribution of Processing Time for Global Path Planning

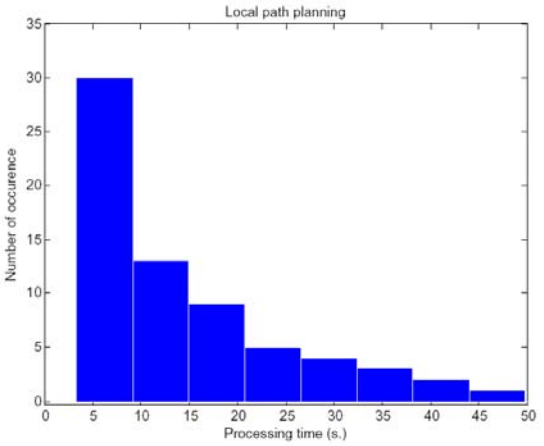

Figure 6 - Statistical Distribution of Processing Time for Local Path Planning for a 10-meter radius

The distribution for the global planning corresponds approximately to a normal distribution except for an anomaly corresponding to paths that were planned into or out of the dense rock field shown at the right of Figure 4. The distribution of the local planning time is approximately a half normal bell shape centered near zero.

5.3. 3D Odometry

To validate the performance of the 3D odometry software, a series of experiments were conducted whereby the rover was asked to perform closed loop trajectories. 29 closed loop trajectories were run to evaluate the performance of the 3D odometry. Tests were stopped when the 3D-odometry indicated that the loop was closed. The actual error was measured using a tape measure at the end of the experiment. The total

distance travelled was computed for each run. The error was computed by taking the difference between the final position and the start position. Percentage errors were computed by dividing the absolute error (in meters) by the path length (also in meters).

Figure 7 and Figure 8 show examples of the logs of the 3D odometry and the wheel odometry. Note that the wheel odometry is expressed in a frame centered at the rover's original pose whereas the 3D odometry is expressed in the terrain global coordinates.

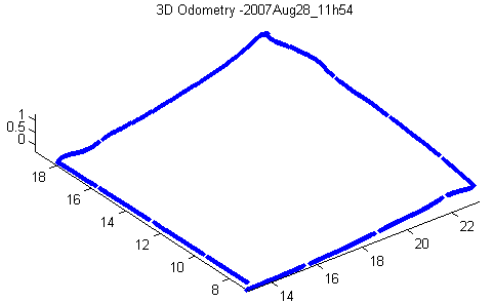

Figure 7 - exp_2007Aug28_11h54m - 3DOdometry

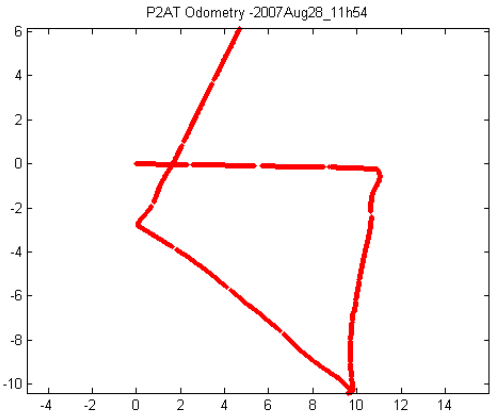

Figure 8 - exp_2007Aug28_11h54m - Wheel Odometry

The results of the statistical error analysis show that the average error observed for wheel odometry alone was on the order of 24.5% with a standard deviation of 18.5%. The maximum error recorded for wheel odometry was 61.13%. This is due to the fact that skid steering introduces very large errors in heading during turns.

The error on 3D odometry had an average of 0.58% with a standard deviation of 0.21%. To gain better insight into the 3D odometry error, it is necessary to decompose it into its horizontal (x-y) and vertical (z) components. The horizontal component is naturally near zero since it is used as the stopping criterion by the robot. The robot assumes that it has completed its trajectory when the horizontal error falls below a given threshold. Since all paths were closed, the vertical error between the end position and the start position is representative of the 3D odometry error due to gyroscope drift. This part of the error can be attributed directly to the 3D odometry algorithms. The vertical error in 3D odometry had an average of 0.51% with a standard deviation of 0.22%.

Finally, the actual error in robot position had an average of 2.19% with a standard deviation of 2.25%. Considering that 3D odometry introduces an error on the order of 0.51% (proportional to vertical component), the error due to wheel slip alone is, on average, on the order of slightly above 1.7%

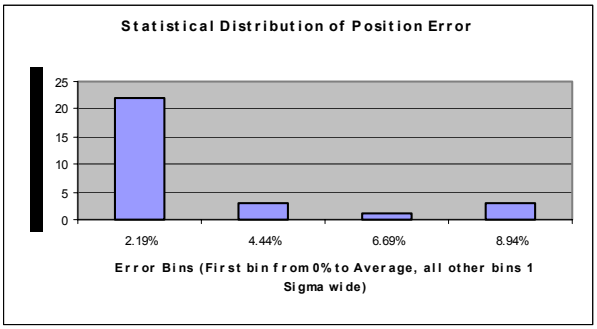

Figure 9 - Performance of 3D Odometry

A histogram of the distribution of the actual error over the experimental runs is provided in Figure 9. It shows that in 22 out of 29 cases (76% of the cases), the error was below the average of 2.19%. Only three cases (10% of the cases) had errors between 2 and 3 sigma above the mean error. These cases are likely due to excessive wheel slip that resulted in large translation errors.

5.4. Semi-Autonomous Traverses

To validate the performance of the integrated system, a series of experiments were conducted in semi-autonomous navigation mode. During these experiments, the rover was commanded to travel from an initial location to a final location beyond the sensing horizon. However, the operator was involved at every step along the way to hand pick via points along the global path in the local terrain scans. The exercised the terrain modelling, local path planning, 3D odometry and rover guidance functionalities. The

global path planning, path segmentation and localisation functions were not used for these tests. The experiments conducted in semi-autonomous mode over the 2006 and 2007 test seasons totalled a few kilometres of distance travelled. Eight runs have been formally logged for a total distance on the order of 800 meters.

All experiments conducted in 2006 and a small fraction of the 2007 experiments were conducted in that mode. Figure 10 (a) shows a summary of a semi-autonomous navigation experiment conducted in 2006. The figure clearly shows that the LIDAR scans have a field-of-view of 40 degrees and a near-field clipping plane at 3 meters. During the experiment, the rover started at the bottom left corner of the image and was commanded to drive around the hill. Destination points were manually picked by the operator in each scan.

Figure 10 (b) to (g) presents a series of snapshots as of the scans as they were collected. Quite prominent are straight lines that were reflected from the boundaries of the Mars terrain. As can be deduced from these lines, during the first three to four scans there was little odometric error accumulated. As the terrain is mainly flat and the robot does not rotate, this was expected. As the rover travelled by the side of the hill, more error was accumulated as can be seen in the scans. It is worth noting that the final scan over an area full of obstacles is quite sparse and has few traversable areas.

5.5. Autonomous Traverses

The final set of experiments are fully autonomous over-the-horizon navigation experiments. These include most the tests that were conducted during the 2007 field campaign. During these experiments, the rover was commanded to travel from an initial location to a final location beyond the sensing horizon. No operator involvement was necessary after the specification of the final destination. These experiments exercised all functionalities: global path planning, terrain modelling, path segmentation, local path planning, 3D odometry and rover guidance. Only scan-based localisation was not tested during these experiments.

During the 2007 test season, 10 such experiments were conducted. The longest autonomous traverse was on the order of 100 meters. The most difficult was conducted through the dense rock field that is visible in the lower right corner of the terrain on Figure 4. The purpose of this last experiment was to stress the system to the limit by imposing a traverse through a field strewn with obstacles sized at the same scale as the rover and with free areas only few rover sizes in width.

Figure 11 shows the sequence of local scans and local paths for a fully autonomous traverse around the hill at the centre of the CSA's Mars Emulation Terrain. For this experiment, the path segmentation algorithm limited the planning horizon to 10 meters for the local scans.

6. Conclusions

This paper presents results of the CSA's autonomous rover navigation research. The 2006 and 2007 field-testing seasons have proven that the general approach and specific algorithms selected can successfully be used for over-the-horizon rover navigation.

The rover's obstacle climbing capability and the sensor height are such that it is approximately at a scale of 1:3 compared to typical exploration rovers. Applying this scaling factor to the 100 meter traverses that were executed, this corresponds roughly to autonomous traverses on the order of 300 meters. This technology could be used to support over-the-horizon traverses on Mars at the scale that is being planned for future missions.

LIDAR sensing has turned out to be very useful for terrain sensing since it provide data with little noise at relatively long range and it is not sensitive to lighting conditions.

The terrain decimation algorithms can successfully reduce the size of a LIDAR point cloud while generally preserving the detailed topography of terrains for conditions that are representative of planetary exploration missions. However, the current algorithm is extremely sensitive to noise: two scans taken from exactly the same location can produce dramatically different mesh. This is due to the presence of noise in the sensor measurement and the fact that the dihedral angle is used as the criterion for choosing the next best decimation target.

The irregular triangular mesh resulting from the decimation of the LIDAR point cloud can successfully be used for path planning to guide a rover through natural terrain.

The integrated experiments have shown that the various technologies developed are compatible with each other and can successfully be used to plan and execute long-range traverses. Fully autonomous and semi-autonomous over-the-horizon traverses of more

than 100 meters were accomplished with in the CSA's Mars emulation terrain.

Comparing the results from the two campaigns, one of the key lessons learned is that the field of view of the terrain sensor is extremely important for path planning and for localization. The 360-degree FOV is much more appropriate for path planning in cluttered environments. However, the 360-degree FOV requires a guided graph search algorithm like A* for path planning to avoid having the planner spend precious time looking for a solution in the opposite direction to the target destination.

Some of the limitations of using a coarse map for global planning and high-resolution terrain scans for local planning have been identified:

It is impossible to plan paths in the global sense going to areas where features are on the scale of the resolution. A good example of such a feature is the canyon in the Mars emulation terrain. Although, there are safe areas for the rover to navigate in the canyon, a coarse map does not have sufficient resolution to find a safe global path. This could be better achieved in semi-autonomous mode.

Furthermore, given that the global path is planned in the coarse map, it is unrealistic to force the robot to follow the global path exactly. Some undetected obstacles can lie on the path. It is sufficient to ensure that the local paths generally follow the global path while tolerating some error.

In the presence of rugged terrain, the terrain model often had very long cast shadows behind obstacles. The resulting terrain model then had very long bridges (looking much like a hand with long fingers). This kind of terrain model is not easily usable to path planning because it contains too many zones of uncertainty. This phenomenon is due to the low incidence angle of the sensor caused by the low sensor placement on the rover. However, raising the sensor only scales the range at which this phenomenon occurs. A capability to assess the terrain model may be required at some point to implement appropriate strategies to deal with these situations in the context of long-range navigation.

Finally, Figure 11 shows the importance of correcting for wheel slip and IMU drift through processes such as visual odometry or scan-to-scan localization. Such a process will be required eventually to complete the implementation of the long-range navigation capability. The impact of wheel slip when conducting traverses through successive local paths is minimal since each local path in planned in a local terrain model. However, global accuracy is important for the rover to correctly reach its final destination. Wheel slip cannot be detected using the current sensor suite and therefore leads directly to position errors at the end of the beyond-the-horizon trajectory.

Current improvement being implemented or planned for the short term future include the development of a more elaborate data structure to store handle multi-layered maps containing different types of data and to integrate them into an atlas. Additional work is also being performed on the meshing to further reduce the memory usage, accelerate processing and reduce sensitivity of the decimation algorithm to noise. The new data structures will be used by a planner that will provide a path consisting not only of line segments but that will also include a safety corridor free of obstacles.

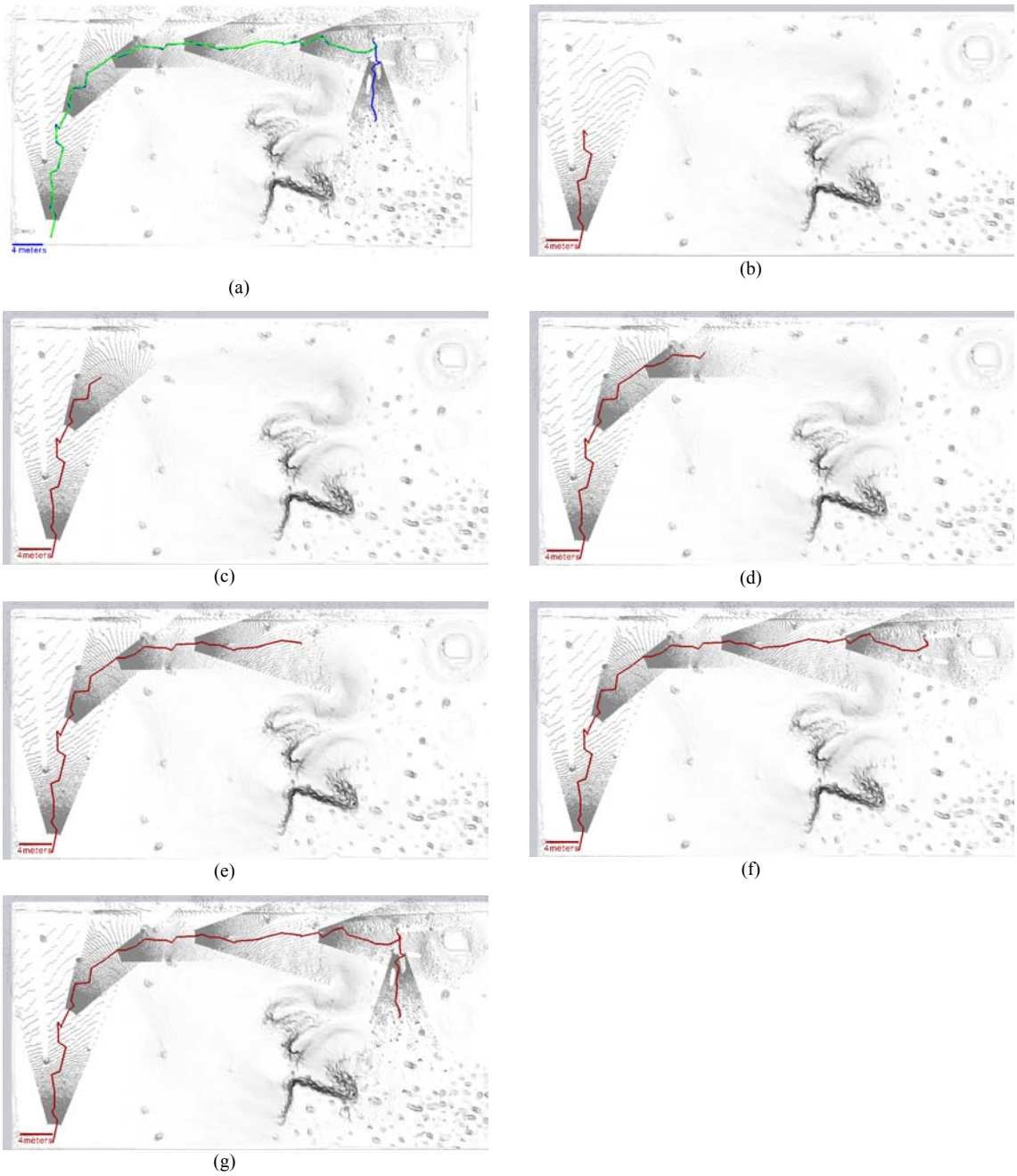

(a) (b) (c) (d) (e) (f) (g)

Figure 10: Semi-autonomous navigation experiment. (a) The scans, the planned paths (blue), and the executed path (green) are overlaid on the Mars emulation terrain model (b) to (g) Cumulative scans and planned paths

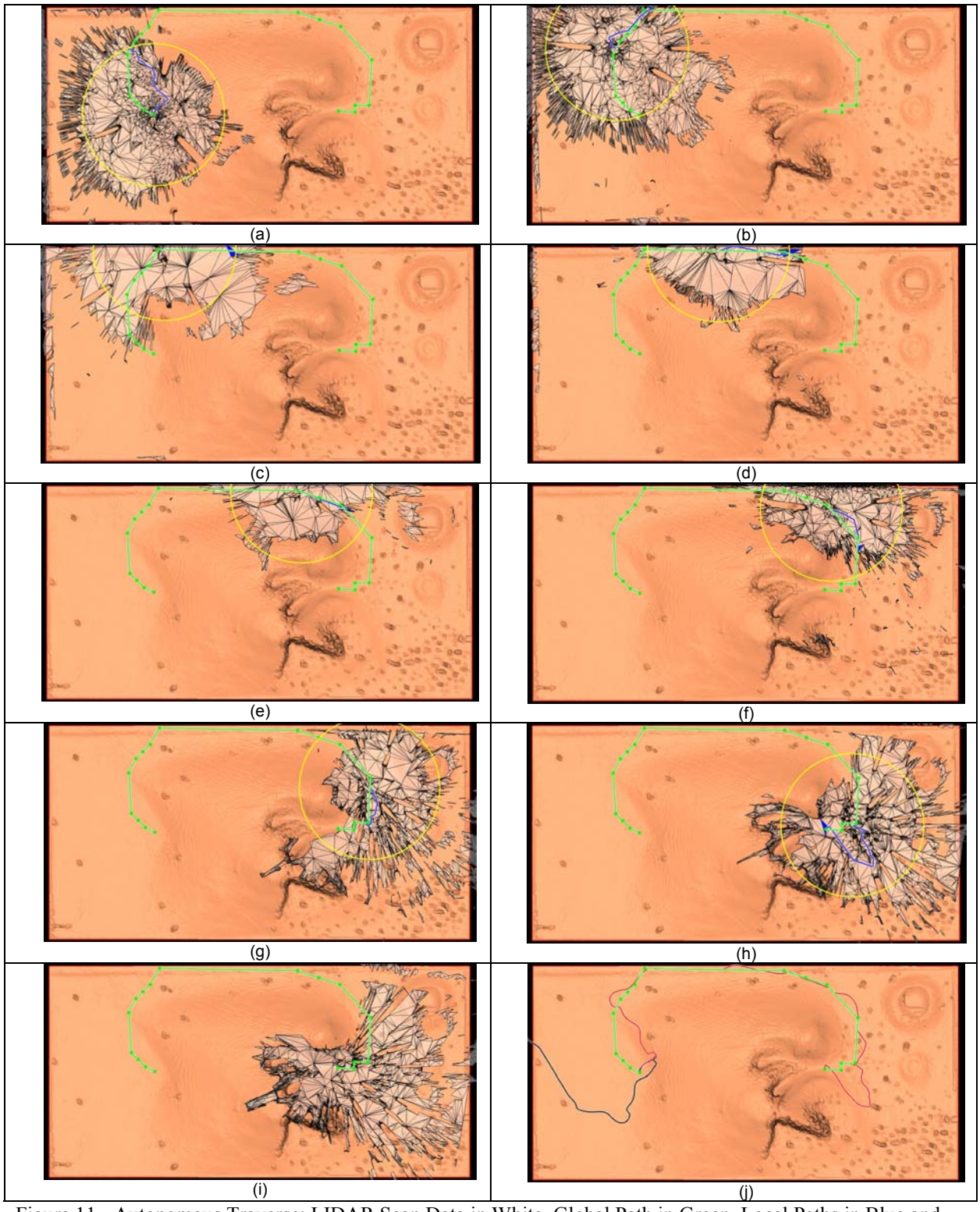

Figure 11 - Autonomous Traverse: LIDAR Scan Data in White, Global Path in Green, Local Paths in Blue and Maximum Planning Horizon in Yellow. Subfigure (j) shows 3D Odometry in Red and Wheel Odometry in Black (Driving off the Chart)

7. References

[1] M. Maimone, J. Biesiadecki, E. Tunstel, Y. Cheng, and C. Leger, Intelligence for Space Robotics. TSI press, 2006, ch. Surface Navigation and Mobility Intelligence on the Mars Exploration Rovers, pp. 45–69.

[2] R. Volpe, "Rover functional autonomy development for the mars mobile science laboratory," in IEEE Aerospace Conf., Big Sky, MT, USA, 2006.

[3] J. Vago, "Overview of exomars mission preparation," in 8th ESA Workshop on Advanced Space Technologies for Robotics & Automation, Noordwijk, The Netherlands, November 2004.

[4] J. Biesiadecki, C. Leger, and M. Maimone, "Tradeoffs between directed and autonomous on the mars exploration rovers," in Procs. Of Int. Symposium of Robotics Research, San Francisco, 2005.

[5] J. Wright, A. Trebi-Ollennu, F. Hartman, B. Cooper, S. Maxwell, J. Yen, and J. Morrison, "Terrain modelling for in-situ activity planning and rehearsal for the mars exploration rovers," in IEEE Int. Conf. On Systems, Man and Cybernetics, vol. 2, 2005, pp. 1372 – 1377.

[6] Johnson, S. Goldberg, C. Yang, and L. Matthies, "Robust and efficient stereo feature tracking for visual odometry," in IEEE International Conference on Robotics and Automation, Pasadena, CA, USA, 19-23 May 2008, pp. 39 – 46.

[7] M. Montemerlo, S. Thrun, H. Dahlkamp, D. Stavens, and S. Strohband, "Winning the darpa grand challenge with an ai robot," in Proceedings of the AAAI National Conference on Artificial Intelligence, Boston, MA, 2006.

[8] D. Wettergreen, N. Cabrol, V. Baskaran, F. Calderon, S. Heys, D. Jonak, R. A. Luders, D. Pane, T. Smith, J. Teza, P. Tompkins, D. Villa, C. Williams, and M. D. Wagner, "Second experiments in the robotic investigation of life in the Atacama desert of Chile," in 8th International Symposium on Artificial Intelligence, Robotics and Automation in Space, September 2005.

[9] A. Kelly et.al., "Toward reliable off-road autonomous vehicles operating in challenging environments," The International Journal of Robotics Research, vol. 25, no. 5-6, pp. 449–483, June 2006.

[10] L. Matthies and S. Shafer, "Error modeling in stereo navigation," IEEE Journal of Robotics and Automation, vol. RA-3, no. 3, pp. 239 – 250, June 1987.

[11] G. Giralt and L. Boissier, "The french planetary rover vap: Concept and current developments," in Procs. of the 1992 IEEE/RSJ Int. Conf. on Intelligent Robots and Systems, vol. 2, 1992, pp. 1391–1398.

[12] Y. Kunii, S. Tsuji, and M. Watari, "Accuracy improvement of shadow range finder: Srf for 3d surface measurement," in Procs. off IEEE/RSJ Int. Conf. on Intelligent Robots and Systems (IROS 2003), vol. 3, 27-31 Oct. 2003, pp. 3041 – 3046.

[13] M. Hebert, C. Caillas, E. Krotkov, I. Kweon, and T. Kanade, "Terrain mapping for a roving planetary explorer," in Proceedings of the IEEE International Conference on Robotics and Automation (ICRA '89), vol. 2, May 1989, pp. 997–1002.

[14] J. Bares, M. Hebert, T. Kanade, E. Krotkov, T. Mitchell, R. Simmons, and W. Whittaker, "Ambler: An autonomous rover for planetary exploration," IEEE Computer, vol. 22, no. 6, pp. 18–26, June 1989.

[15] S. Goldberg, M. Maimone, and L. Matthies, "Stereo vision and rover navigation software for planetary exploration," in IEEE Aerospace conference proceedings, vol. 5, Big Sky, Montana, USA, March 2002, pp. 2025–2036.

[16] S. Ruel, D. Ouellet, T. Luu and D. Laurendeau, Automatic Tracking from TriDAR daat for Autonoumous Rendezvous and Docking, 9th International Symposium on Artificial Intelligence, Robotics and Automation in Space, Pasadena, February 2008.

[17] R. J. Fowler and J. J. Little, "Automatic extraction of irregular network digital terrain models," in SIGGRAPH '79: Procs. of the 6th annual conference on Computer graphics & interactive techniques, 1979, pp. 199–207.

[18] Rekleitis, J.-L. Bedwani, S. Gemme, and E. Dupuis, "Terrain modelling for planetary exploration," in Computer and Robot Vision (CRV), Montreal, Quebec, Canada, May 2007, pp. 243–249.

[19] Rekleitis, J.-L. Bedwani, E. Dupuis, and P. Allard, "Path planning for planetary exploration," in Fifth Canadian Conference on Computer and Robot Vision (CRV), Windsor, Ontario, 28-30 May 2008, pp. 61– 68.

[20] Nsasi Bakambu, J., Gemme, S. and Dupuis, E., "Rover Localisation through 3D Terrain Registration in Natural Environments", 2006 IEEE/RSJ International Conference on Intelligent Robots and Systems, Beijing, China, October 2006.